Heliyon 10 (2024) e40559

Contents lists available at ScienceDirect

Heliyon

journal homepage: www.cell.com/heliyon

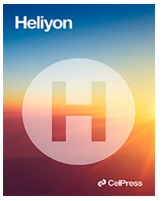

Research article

Interspecies transcriptome profiles of human T cell activation and liver inflammation in a xenogeneic graft-versus-host disease model

Seo Yule Jeong [a], Duhyeon Park [b], Tamina Park [b], Ji-Seok Han [a], Jungyun Lee [a], Chang Hoon Choi [a], Minseong Jo [a], Yu Bin Lee [a], Mi-lang Kyun [a], Myeongjin Choi [a,***], Daeui Park [b,**], Kyoung-Sik Moon [a,*]

[a] Department of Advanced Toxicology Research, Korea Institute of Toxicology, Daejeon, 34114, Republic of Korea
[b] Department of Predictive Toxicology, Korea Institute of Toxicology, Daejeon, 34114, Republic of Korea

ARTICLE INFO

Keywords:
Graft-versus-host disease
Humanized mouse model
T cell pathway
Liver toxicity
Transcriptome analysis

ABSTRACT

Background: Xenogeneic transplantation induces acute graft-versus-host disease (aGvHD) and subsequent vital organ damage. Herein, we aimed to examine hepatic damage associated with aGvHD using histopathology and gene expression profiles.

Methods: A xenografic GvHD model was established by engrafting human peripheral blood mononuclear cells (PBMCs) into immunodeficient NOD-scid IL2Rγnull (NSG) mice after busulfan conditioning. NSG mice were assigned to groups treated with saline (S group) or a combination of busulfan and PBMCs (BP group). Histological lesions and RNA sequencing analysis of gene profiles in the BP group (GvHD model) were compared with those in the P group.

Results: Predominant T cell subsets (95 %) in the blood of the BP group were identified as cytotoxic $CD8^+$ T cells (56 %) and helper $CD4^+$ T cells (31 %). Symptoms of aGvHD, including hepatocyte necrosis, bile duct hyperplasia, and human T cell infiltration, were observed. Gene expression analysis revealed upregulation of Th1 and Th2 cell differentiation (*STAT4, IL4R,* and *NFACT1*), T cell receptor signaling pathway (*CD226* and *GBP1*), IL-1 pathway (*CCL3, NAIP,* and *IRAK4*), cell cycle (*CDCA5, CDCA8, MCM5, KNL1, BUB1B, FBXO5,* and *CENPE*) in human cells. In mouse cells, *Il1a*, *Ifngr*, *Tnfrsf*, and *Il6ra* genes (cytokines or their receptors) and *Icam*, *Vcam*, and *Endra* genes (adhesion molecules) were upregulated, whereas genes related to chromosome condensation (*H2ac* and *H2bc*) and fatty acid/steroid metabolism (*Fasn*, *Rdh*, and *Scd*) were downregulated. Interspecies gene network analysis revealed that activated human T cells are associated with liver damage through inflammatory and metabolic pathways, accompanied by increased mouse cell adhesion molecules and cytokines.

Conclusion: Our findings offer valuable insights into the pathophysiology and biomarkers of aGvHD and may contribute to the development of novel therapeutics.

Abbreviations: PBMC, peripheral blood mononuclear cells; HSC, hematopoietic stem cells; ELISA, enzyme-linked immunosorbent assay; NSG, NOD/LtSz-scid IL-2Rg null; GvHD, graft versus host disease; IHC staining, immunohistochemistry staining; CyTOF, cytometry by time of flight; Treg, regulatory T cells; AST, aspartate aminotransferase; ALT, alanine aminotransferase..

* Corresponding author. Korea Institute of Toxicology, 141 Gajeong-ro, Yuseong-gu, Daejeon, 34114, Republic of Korea.
** Corresponding author. Korea Institute of Toxicology, 141 Gajeong-ro, Yuseong-gu, Daejeon, 34114, Republic of Korea.
*** Corresponding author. Korea Institute of Toxicology, 141 Gajeong-ro, Yuseong-gu, Daejeon, 34114, Republic of Korea.
E-mail addresses: myeongjin.choi@kitox.re.kr (M. Choi), daeui.park@kitox.re.kr (D. Park), ksmoon@kitox.re.kr (K.-S. Moon).

https://doi.org/10.1016/j.heliyon.2024.e40559
Received 12 September 2024; Received in revised form 18 November 2024; Accepted 18 November 2024
Available online 28 November 2024

1. Introduction

Graft-versus-host disease (GvHD) occurs when transplanted immune cells attack the recipient's tissues. This condition can develop after allogeneic or xenogeneic transplantation involving peripheral blood mononuclear cells (PBMCs), stem cells, or bone marrow [1,2].

GvHD can be either acute or chronic. Classic acute GvHD (aGvHD) develops within the first 100 days after transplantation and is typically characterized by clinical signs such as rash, nausea, anorexia, diarrhea, or cholestatic liver damage [3,4]. Classic chronic GvHD (cGvHD) can occur without time constraints and does not present with acute GvHD symptoms. Notably, cGvHD is predominantly characterized by features such as poikiloderma, esophageal web, bronchiolitis obliterans, and scleroderma or scleroderma-like syndromes [2,5].

Both acute and chronic GvHD require careful management with immunosuppressants and supportive care. GvHD leads to tissue damage, impaired immune function, treatment difficulties, and an increased risk of cancer recurrence [3]. Therefore, GvHD can substantially impact the quality of life and long-term outcomes in transplant recipients, and these can be improved through early detection and intervention [6].

Humanized mice are developed from immunodeficient mice that have been genetically altered or bred to lack specific immune components [2,7–9]. For example, the NOD-scid IL2Rgamma-null mouse (NSG), commonly used in humanized mouse research, was created through genetic modifications combining the NOD phenotype with severe combined immunodeficiency (SCID) and an interleukin (IL) 2 receptor gamma chain (Il2rg) knockout. In this strain, the absence of T, B, and natural killer (NK) cells, along with defective dendritic cells and macrophages, results in deficiencies in both innate and adaptive immune systems [10,11]. Immunodeficient mice can be engrafted with human PBMCs to mimic the human immune system. Additionally, to further suppress their immune systems before engraftment, immunodeficient mice are treated with a combination of radiation and/or busulfan. The doses vary depending on experimental requirements, ranging from 0.85 to 5 Gy for radiation and 25–40 mg/kg for busulfan [12–14].

Mouse models of xenogeneic GvHD exhibit symptoms such as weight loss, skin changes, diarrhea, hepatomegaly (enlarged liver), splenomegaly (enlarged spleen), lethargy, hunched posture, and, in severe cases, mortality. In humanized mouse models, xenogeneic GvHD can develop depending on the PBMC donor, the total PBMC number, the injection route, and the preconditioning treatment (irradiation or chemotherapy) [15]. Although this model does not fully replicate the symptoms observed in human GvHD, it provides valuable insights into GvHD mechanisms and potential therapeutic approaches [2,16,17]. Histopathologic features observed in the liver, gastrointestinal tract, and lungs of xenogeneic GvHD mice include disorders such as hepatitis, liver necrosis, intestinal enteritis, and lung alveolar damage.

The characteristic features of hepatic GvHD include damage to hepatocytes and the biliary endothelium, with cellular infiltration around the portal vein in human and mouse [18–20]. Infiltrating T-cell-induced inflammation causes hepatic injury via Fas-Fas ligand (FasL), perforin/granzyme, and tumor necrosis factor (TNF)-TNF receptor binding in patients [3]. Elevated pro-inflammatory cytokines, including TNF superfamily, interleukin-1 family (IL-1), and interferon-gamma were reported in allogeneic and xenogeneic transplanted mice [16,21]. Biomarkers including tumor necrosis factor receptor 1 (TNFR1), IL-2 receptor alpha (IL-2RA), and soluble IL-33 receptor have been used to predict prognosis and diagnose acute GvHD in patients [3]. As low TNFR1 amounts are associated with better outcomes, TNF superfamily blockers have been used to prevent GvHD in high-risk patients who underwent hematopoietic stem cell transplantation [3,22].

Given the elevated aspartate aminotransferase (AST) concentration in the blood of mice suffering from xenograft GvHD, our primary focus was to investigate liver damage induced by the condition. The histopathological symptoms of liver damage caused by xenografic GvHD and the expression levels of damage-related genes were explored using RNA sequencing (RNA-seq) analysis. To our knowledge, this is the first report to show transcriptome profiling of immune cells and liver tissue in a humanized model suffering from GVHD following busulfan conditioning. These results will provide an important basis for establishing novel therapeutics for treating aGvHD in patients.

2. Materials and methods

2.1. Animals

Six-week-old female NOD.Cg-*Prkdc*^{scid} *Il2rg*^{tm1Wjl}/SzJ (NSG) mice were purchased from Jackson Laboratory (Bar Harbor, ME, USA) and allowed to acclimate for 10 days. The mice were randomly assigned to one of four groups. All mice were housed under the following conditions: a temperature of 22 ± 1 °C, 55 ± 10 % humidity, and a 12 h light: dark cycle (5 adult mice/cage). One animal technical staff member was informed of the group allocation for blind analysis. This study was approved by the Institutional Animal Care and Use Committee (IACUC No. 2112–0079, Korea Institute of Toxicology). Throughout the experiments, the mice were observed daily. All protocols were designed to minimize the number of animals and their pain or distress, in accordance with the relevant regulations. The ARRIVE guidelines were used in this study.

2.2. Engraftment of human PBMC in NSG mice

Six-week-old female NSG mice were allocated to each of the four groups. In the BP and B groups, mice were administered 25 mg/kg busulfan (intraperitoneal injection)(Otsuka America Pharmaceutical, Japan) on day −1 and −2 with or without post-PBMC treatment

(intravenous injection), respectively (Fig. 1A). In group P, mice were treated with human PBMC alone on day 0. Mice treated with the vehicle (saline) were assigned to the S group (Supplementary Table 1). PBMCs from a healthy donor (#CC-2702, 35 years old, male, Hispanic, USA) were obtained from Lonza (Basel, Switzerland). PBMC was negative for human immunodeficiency virus, hepatitis B virus, and hepatitis C virus. Cryopreserved PBMCs were thawed in a water bath at 37 °C and washed twice with PBS by centrifugation. PBMCs were resuspended in RPMI 1640 medium and injected into mice at 2×10^5 PBMCs (83.3 % of which were $CD3^+$ cells) on day 0. Busulfan and PBMC were administered to mice via intraperitoneal and intravenous injection, respectively. The animal experiment was terminated on onset of GvHD (day 21), at which point all animals in the BP group were alive and showed clinical signs of GvHD, including decreased body weight and activity, ruffled fur, and alopecia, as reported in previous studies [1,23]. The order of the treatments and measurements was recorded. The weights of mice were measured once a week.

2.3. Blood analysis

Blood samples from the inferior vena cava were collected into K2-EDTA tubes. To analyze liver damage markers including AST, and alanine aminotransferase (ALT), blood was centrifuged at 2,000g for 10 min to collect serum. The parameters were evaluated using a Toshiba 120FR chemistry analyzer (Toshiba Medical System, Tokyo, Japan). For flow cytometry analysis, cells were lysed with RBC lysis buffer (BioLegend, San Diego, CA, USA) and stained with specific human antibodies. All samples were analyzed using a Cytoflex S flow cytometer (Beckman Coulter, USA) and stained with the specific antibodies listed in Supplementary Table 2, according to the manufacturer's instructions. Data were analyzed using CytExpert Software v2.4 and Kaluza v. 2.2 (Beckman coulter, Brea, CA, USA). The following cellular phenotypes were determined: leukocytes ($hCD45^+$), T cells ($hCD3^+/hCD45^+$), cytotoxic T cells ($hCD8^+/hCD3^+/hCD45^+$), and helper T cells ($hCD4^+/hCD3^+/hCD45^+$).

2.4. Liver weight and histopathology

Liver samples from all mice were collected and weighed. The ratio of liver to body weight was also calculated. Liver samples were fixed in 5 % formalin and embedded in paraffin. Tissues were cut into 5-μm thick slices and stained with hematoxylin & eosin. GvHD lesions were evaluated for the level of inflammation, bile duct damage, ballooning, fibrosis, and necrosis [20,24] by a board certified pathologist using blind tests as follows: 0 (absent), 1 (minimal), 2 (mild), 3 (moderate), 4 (marked), and 5 (severe) to obtain the

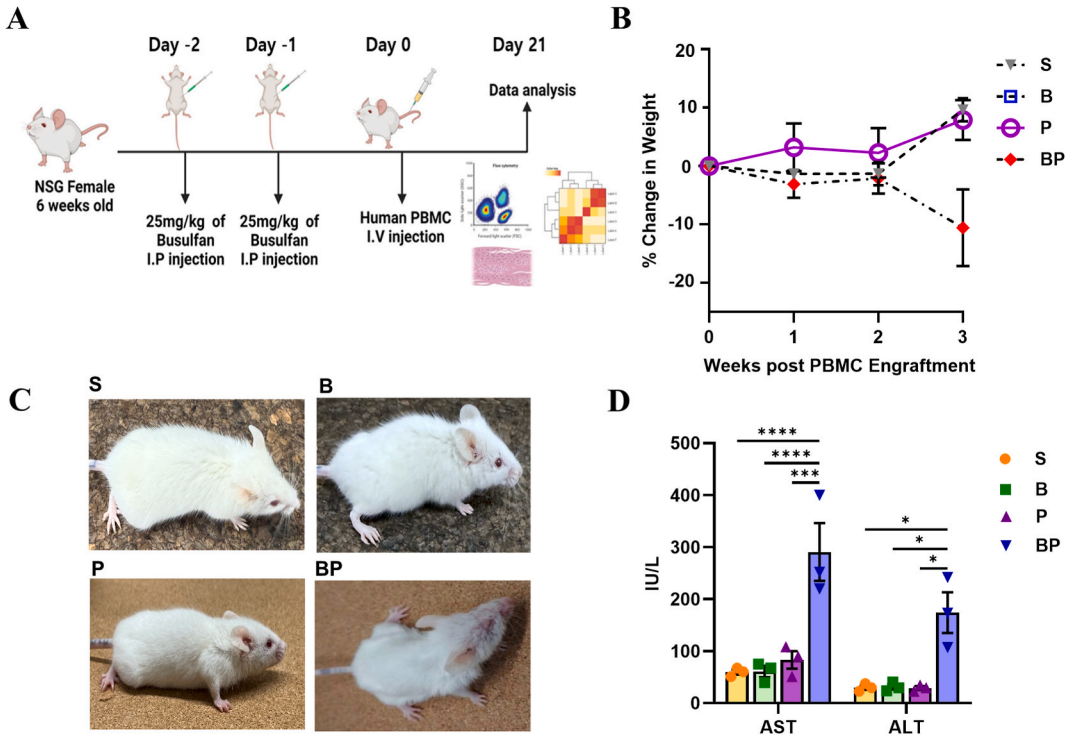

Fig. 1. Scheme for the generation of acute GvHD model. (A) Experimental scheme for BP group. NSG mice received two doses of busulfan at 25 mg/kg intraperitoneally prior to human PBMC injection. Clinical GvHD signs were observed 3 weeks after PBMC administration. (B) The mean percentage change in body weight over 3 weeks after intravenous administration of PBMCs (P group, n = 3; BP group, n = 3) or without PBMCs (S group, n = 3; B group, n = 3). (C) Clinical signs of GvHD. Symptoms including hunching posture, decreased activity, reduced body weight, ruffled fur, and hair loss were observed in the BP group. (D) Clinical liver injury markers, including AST and ALT, were analyzed in the serum of three mice in all groups. N = 3. All values represent mean ± S.E.M. $*p < 0.05$, $***p < 0.001$, $****p < 0.0001$ according to one-way ANOVA.

inflammatory score. To detect infiltrating human $CD3^+$ T cells, immunohistochemistry (IHC) staining was performed with 0.03 % H_2O_2 and Tris-EDTA buffer for antigen retrieval. Staining was conducted with a polyclonal human anti-CD3 antibody (Abcam, Cambridge, UK, #ab828) and a HRP-conjugated anti-rabbit secondary antibody (Dako,US, #K4003). Histological examination was conducted in a blind manner. The percentage of stained area was estimated using ZEN software. All slides were examined histologically using an AxioScan Z1 slide scanner (Goettingen, Germany).

2.5. High throughput sequencing of mouse liver tissues with infiltrated human PBMCs

Total RNA was extracted from mouse liver tissues in each group using the RNeasy Mini Kit (Qiagen, Hilden, Germany). The RNA-seq library was generated using the TruSeq Stranded mRNA Library Prep Kit, according to the manufacturer's instructions (Illumina, San Diego, CA, USA). Using the Illumina NovaSeq 6000, 101 bp paired-end sequencing reads were obtained. To conduct interspecies transcriptome analysis, two reference genome sequences of *Homo sapiens* (GRCh38.p14) and *Mus musculus* (GRCm39) were aligned using STAR version 2.7.10a and XenofilteR version 1.6 [25,26]. XenofilteR is an R package that generates filtered results for host and recipient by classifying sequencing reads aligned to both genomes using STAR as mouse or human, based on whether the gene had more mismatches in the two reference sequences. The abundance of filtered genes was calculated from the number of mapped reads using featureCounts in Subread version 2.0.3 [27]. Using the read counts and counts per million (CPM), the genes were quantified for each condition in edgeR [28]. Differentially expressed genes (DEGs) were selected based on a fold change greater than two-fold, with a false discovery rate (FDR) of less than 0.05.

2.6. Multidimensional scaling

The level of similarity between samples was represented in a two-dimensional space using multidimensional scaling (MDS) between gene expression profiles. The dissimilarity between 11 samples, based on normalized gene expression profiles, was calculated as the Manhattan distance using the cmdscale in the stats R package.

2.7. Gene set enrichment analysis and heatmap of significant pathways

Based on the DEGs obtained using edgeR, the Metascape and Enrichr web portals were used for gene set enrichment analysis (GSEA) [29,30]. GSEA effectively selected significant biological pathways from the DEGs. The cumulative hypergeometric statistical test was used to determine the statistically significant value (*p*-value) for each biological pathway, which was converted to -log (*p*-value). Heatmaps and boxplots were used to illustrate the gene expression values of significant pathways. The Euclidean distance and central connectivity under each experimental condition were determined using an agglomerative approach for hierarchical clustering. Heatmaps were obtained using the heatmap.2 R package. In the box plot, the gene expression levels in each experimental group were ascertained using stat_compare_means with a paired *t*-test from the ggpubr package. A p-value <0.05 indicated statistical significance. Pearson correlation was calculated between mouse liver inflammation scores and the expression level of human genes related to the cell cycle, IL1, T cell pathway.

2.8. Construction of network between human T cells and mouse pathways

To examine pathophysiologic interactions between human DEGs and mouse DEGs, a biological pathway network was constructed using Metascape based on the upregulated genes. In the network, nodes represent significant pathways and the edges represent the interactions of pathways. The edges were generated by shared genes between nodes. When the number of shared genes is increased, the thickness of edges also increases in the network. Shared genes in this context were genes that participate in multiple pathways or processes, indicated by edges connecting different nodes. These shared genes were significant as they highlight functional connections between pathways, often serving as a key gene. Based on shared genes between DEGs of two species, we performed the functional connections between humans and mice.

2.9. Statistical analysis

All data were obtained from live animals (n = 2–5/group). Data generated from the same experiment set were presented as average ± SEM. To investigate the correlation between inflammation scores and gene expression levels, five mice in the BP group were included for RNA-seq analysis. Statistical analyses were performed using GraphPad Prism Version 9.3.1 software (GraphPad software, USA). One-way ANOVA was used to compare the four groups in this study. Comparisons between the P and BP groups (n = 7–10/group) were analyzed using Student's *t*-test. Statistical significance was set at p-value <0.05. The p-values less than 0.001 were represented with three asterisks (***), while the p-values less than 0.0001 were marked with four asterisks.

3. Results

3.1. Establishment of the acute GvHD model

To induce xenogeneic aGvHD in a humanized mouse model, the BP group was administered with myeloablative conditioning using

busulfan followed by PBMCs engraftment (Fig. 1A). The S group was treated with saline alone. To rule out the effects of busulfan or PBMC administration, mice were assigned to either the B group, which received only busulfan, or the P group, which received only PBMCs. To investigate liver injury in humanized mice with signs of aGvHD, the animal experiment was terminated on day 21, during which the BP group exhibited acute GvHD symptoms. Over 3 weeks after PBMC engraftment, no significant change in body weight was observed among the groups, as shown in Fig. 1B. However, a decreased body weight by approximately 10.6 % was observed in BP groups unlike in the other groups. Three weeks after PBMC injection, body weights increased by 9.6 %, 10.9 %, and 7.9 % in the S, B, and P groups, respectively. Additionally, the BP group exhibited typical signs of acute GvHD, such as a hunching posture, mild-to-moderate decrease in activity, and ruffled fur with alopecia around the nose, distinguishing it from the other groups (Fig. 1C). In blood biochemistry analysis, significantly elevated AST and ALT amounts were observed in the serum of the BP group compared with other groups (Fig. 1D).

3.2. Engrafted human immune cells in mouse blood

Samples were gated on live and single cells using SSC-H/FSC-H and FSC-H/FSC-A gating, respectively (Supplementary Fig. 1). The viability of all samples was more than 90 % (Vi-CELL, Beckman Coulter). The human immune cell gating technique was used to identify engrafted human leukocytes (hCD45+), T cells (hCD3+), and T cell subsets (hCD4+ and hCD8+) as shown in Fig. 2A and B. The full gating strategy was provided in Supplementary Fig. 1. Flow cytometry analysis was performed for the all groups. In the BP group, a significant increase in the percentage of engrafted human leukocytes (46.7 %) in total leukocytes was observed compared to that in other groups (Fig. 2C). In contrast, human leukocytes in total leukocytes of group P were engrafted in extremely low proportions (1.5 %). In the BP group, the percentage of hCD3+ cells in engrafted human leukocytes (hCD45+) was 95 %, whereas these cells were not detected in the other groups (Fig. 2D). In addition, the T cell subsets in total T cells of the BP group were identified as cytotoxic T cells (hCD8+, 56 %) and helper T cells (hCD4+, 31 %) (Fig. 2E).

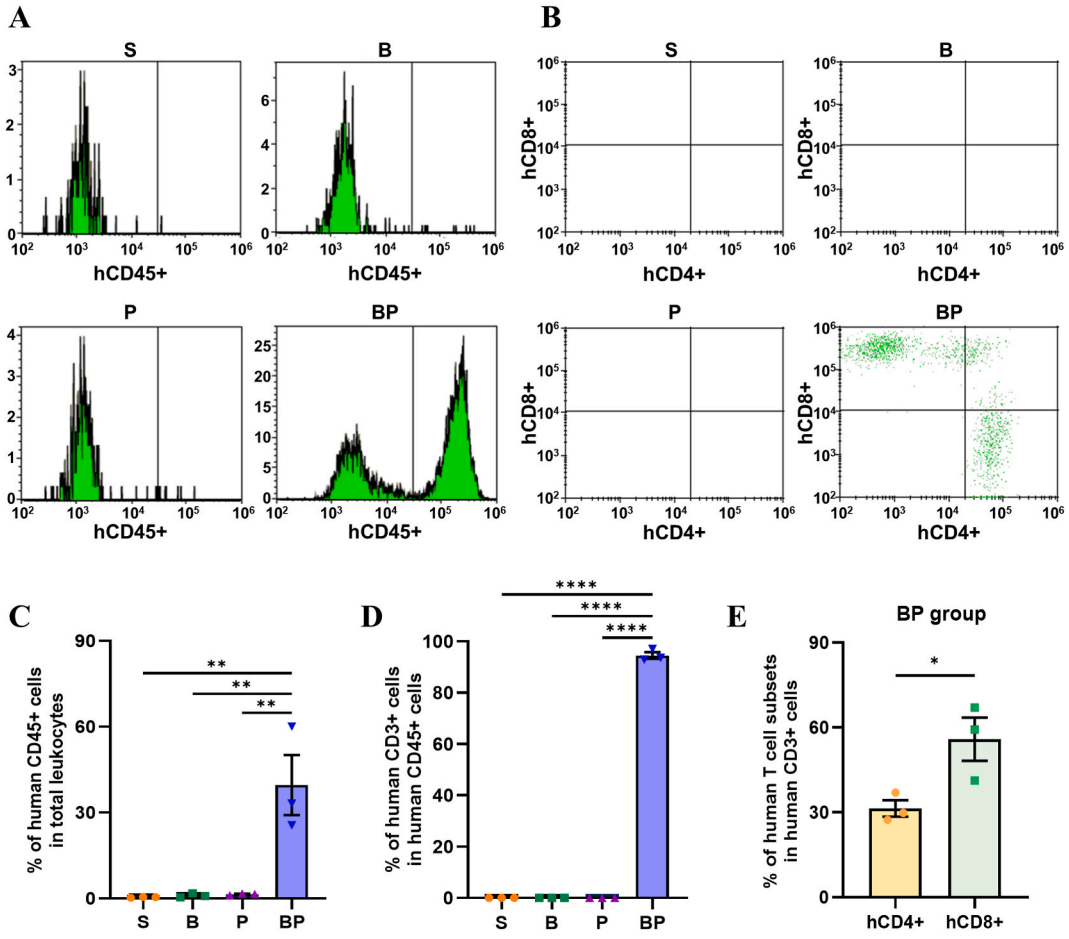

Fig. 2. Characterization of engrafted human cells in the peripheral blood obtained from mice at day 21. (A) The mean percentage of human $CD45^+$ cells in total leukocyte of mice. (B) The mean percentage of human $CD3^+$ cells in human $CD45^+$ cells of mice. (C) The subpopulations of human $CD3^+$ T cells ($CD4^+$ helper T cells and $CD8^+$ cytotoxic T cells) in human $CD3^+$ cells were calculated. All values represent mean ± S.E.M. $*p < 0.05$, $**p < 0.01$, and $***p < 0.001$ according to student's t-test and one-way ANOVA. n = 3.

3.3. Liver weight and histopathological examination

The liver-to-body weight ratio was significantly higher in the BP group compared to the P group (p-value <0.05) (Fig. 3A), with the BP group having a ratio of 7.1 %, while the ratio in the S, B, and P groups ranged from 4.3 % to 4.5 %. The histopathological morphology of liver tissue in the BP group was compared with that in the other groups (Fig. 3B). Infiltration of inflammatory cells around the portal vein, hepatic artery, and bile duct was high in the BP group (white arrow) and mild in the P group. Further, single hepatocyte necrosis (yellow circle), characterized by a condensed hypereosinophilic cytoplasm with a round or angular outline and fragments of nuclear material, was observed multifocally in the hepatic parenchyma with or without inflammatory cell infiltration. Bile duct proliferation (black arrow) was also observed in the portal area, with mixed infiltration by human immune cells. Damaged bile duct epithelium with overlapping nuclei was found in the liver and was associated with evidence of hepatic injury and repair resulting from bile flow obstruction. As shown in the control image (S) on the upper right (Fig. 3B), the liver sinusoids are usually empty (black circle) under normal conditions, and Kupffer cells are rarely observed. However, in the image on right below, Kupffer cells with faint basophilic cytoplasm can be seen multifocally within the sinusoids (blue circle). The degree of inflammation was scored and plotted as shown in Fig. 3C and Supplementary Table 3. The liver inflammatory score was significantly higher (3-fold) in the BP group than that in the P group. In the IHC staining analysis, hCD3+ T cells were observed around the portal vein in the liver of both the P and BP groups. (Fig. 4A). The intensity of IHC staining was significantly higher (by 3.2-fold) in the BP group compared to the P group (Fig. 4B).

3.4. Gene expression profile of liver tissue in the GvHD model

For gene expression analysis in the GvHD model, it is crucial to differentiate between sequencing reads of human and mouse genes, as the mRNA is sourced from both mouse liver and human PBMCs. Therefore, we used XenofilteR. The alignment results of the human and mouse genomes before and after filtering were stored in binary alignment map (BAM) files. The number of mapped reads was determined and used to indicate the gene expression trends in both human and mouse (Fig. 5A). In the analysis, the total number of reads from our samples was produced as an average 78 million (68–93 million). In addition, the number of human mapping reads was mapped as an average 3.01 % (1.14–5.42 %). XenofilteR distinguished between the sequencing reads of the two species well. To visualize the relationships between samples, an MDS plot was generated using gene expression profiles aligned to the *Mus musculus* reference genome (Fig. 5B). The MDS plot represents the gene expression profiles of S (n = 2), B (n = 2), P (n = 2), and BP (n = 5) groups at 11 points. The points were organized according to the MDS plot based on the Manhattan distances between each pair of samples. These distances indicated the degree of dissimilarity in terms of variance for the entire dataset. The results of the two-dimensional reduction showed that each group was separated from the other (Fig. 5B). The G2-16 sample displayed a different

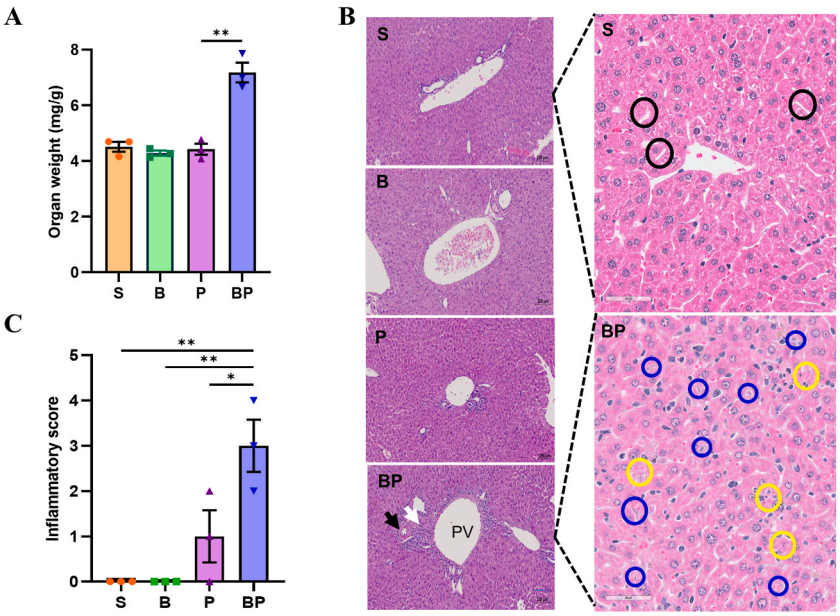

Fig. 3. Liver weight and histopathological examination. (A) The ratio of liver weight to body weight (mg/g) was calculated for mice 3 weeks after PBMC administration. (B) Histopathological evaluation of liver tissues with H&E staining. Infiltrating immune cells were observed around the portal vein (PV), hepatic artery (HA), and bile duct (BD) in the liver of BP group mice (white arrow, n = 3). The black arrow indicates bile duct hyperplasia. The blue and yellow circles highlight Kupffer cell hyperplasia and hepatic necrosis, respectively. (C) Infiltration of inflammatory cells was scored as 0 (absent), 1 (minimal), 2 (mild), 3 (moderate), 4 (marked), or 5 (severe). All values represent mean ± S.E.M. *$p < 0.05$, and **$p < 0.01$ according to one-way ANOVA. n = 3.

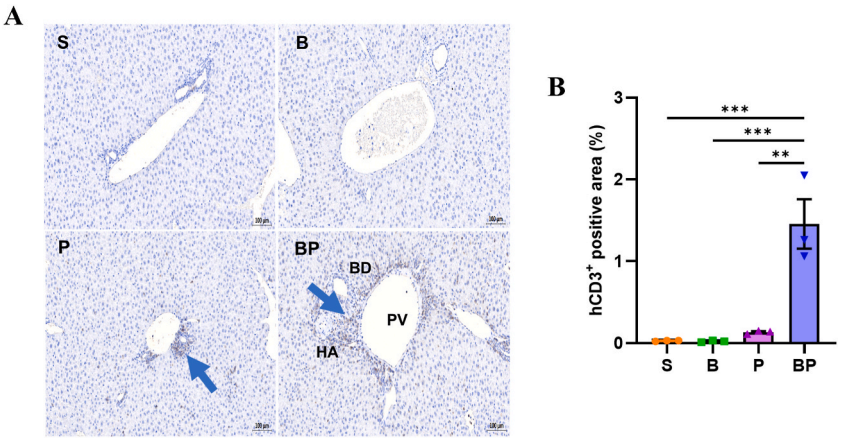

Fig. 4. Immunohistological staining of the liver from hPBMC-engrafted mice. (A) Immunohistochemistry for $CD3^+$ cells highlights infiltrated human T cells (blue arrow) around the portal vein (PV) and hepatic artery (HA). (B) The relative stained area of $CD3^+$ cells was quantified as a proportion of the total area. All values represent mean ± S.E.M. $^{**}p < 0.01$ according to one-way ANOVA. n = 3.

pattern with distance compared to the other samples because the G2-16 sample (liver inflammatory score:3) had a more severe inflammatory score than that of the other samples (Supplementary Table 3).

DEGs were defined as upregulated or downregulated genes with a greater than or less than 2-fold change under conditions with FDR less than 0.05. From the human mapping results, 137 genes were upregulated and 195 downregulated in the BP group compared to those in the P group (Supplementary Table 4–1). From the mouse mapping results, 53 DEGs were upregulated and 50 DEGs were downregulated in the B group when compared to those in the S group, and 1027 DEGs were upregulated and 274 DEGs were downregulated in the BP group compared to those in the S group (Fig. 5C and Supplementary Table 4–2). The number of DEGs in the BP group was larger than in both the B and P groups. In particular, the number of upregulated genes was approximately 3.7-fold those of the downregulated genes in the BP group (Fig. 5C).

The distribution of DEGs under each condition was visualized using MA plots and volcano plots (Fig. 5D–F). In the MA plot, MA represents M and A values. The M value on the Y-axis represents the logarithm of the expression level ratio, and the A value on the X-axis represents the logarithm of the normalized levels of gene expression, also known as CPM. The DEGs in the GvHD model (BP group) were more abundant than in the other groups.

3.5. T cell differentiation in infiltrating human PBMCs

To understand the DEGs of human, gene set enrichment analysis provided by Enrichr utilized 137 upregulated and 195 downregulated genes. The upregulated genes were involved in T cell pathway, including T cell receptor signaling pathway, Th1 and Th2 cell differentiation (Fig. 6A and Supplementary Table 4–3). Human-oriented genes such as *CD226* ($\log_2$ fold-change($\log_2$FC) = 1.5), *GBP1* (2.2), *IL4R* (2.0), *STAT4* (1.3), and *NFATC1* (2.3) were enriched in the T cell pathways (Fig. 6B and Supplementary Table 3). Also, upregulated human genes associated with IL-1 were detected in the BP group such as *GBP5* (3.2), *PYHIN1* (3.1), *CCL3* (4.6), *NAIP* (2.7), *IRAK4* (1.6), and *MAP3K7* (3.3) (Supplementary Table 4–3). The upregulation of T cell-related genes was well supported by the levels of human $CD4^+$ and $CD8^+$ T cells (Fig. 2E), as well as the infiltration of human PBMCs in the mouse liver pathology of the BP group (Fig. 3B). Interestingly, G2-14 mice in the BP group did not show increased expression of genes associated with T cell activation (Fig. 6B), which suggests that their mild inflammation symptoms may be related to this lack of gene upregulation. On the contrary, T cell pathway-related genes were more upregulated in the G2-16 mouse with a severe inflammation score than in the other mice. This implies the expression pattern was closely correlated with the liver inflammatory score of each mouse (Fig. 6C).

In addition, biological pathways related to the cell cycle were particularly prevalent such as *CDCA5* (3.4), *CDCA8* (5.2), *MCM5* (3.2), *KNL1* (2.1), *BUB1B* (2.1), *FBXO5* (1.7), and *CENPE* (1.6). In our model, the upregulated pathways showed an overall trend related to T cell infiltration by upregulation of cell cycle. The information on genes is described in Supplementary Table 4–3. Reprogramming of cellular metabolism is a feature of GvHD, which is associated with differentiation of hCD4+ cells into the pathogenic Th1 subset, along with dysfunction of immune-suppressive protective T regulatory cells (Tregs). We performed a correlation analysis to examine the relationships between the expression levels of human genes associated with T cell pathway and the inflammatory scores, as well as between the expression levels of genes related to cell cycle and IL-1 pathway and the inflammatory scores in the aGvHD model (Fig. 6C–E and Supplementary Table 4–4). Interestingly, as the inflammatory response in the aGVHD model increased notably, genes associated with T cell pathway, IL-1, and cell cycle were also upregulated. The Pearson correlation score between the mouse liver inflammatory scores and the human gene expressions of T cell pathway (5 genes) and cell cycle pathway (16 genes), and IL-1 pathway (6 genes) showed an average of 0.91. There was a high correlation between each mouse liver inflammation score and human gene expression pattern. Some of these genes were selected and visualized in correlation with the inflammation score of the mouse liver (red shapes) in Fig. 6D and E. The gene expression between the S and BP groups was significantly different (all *p*-

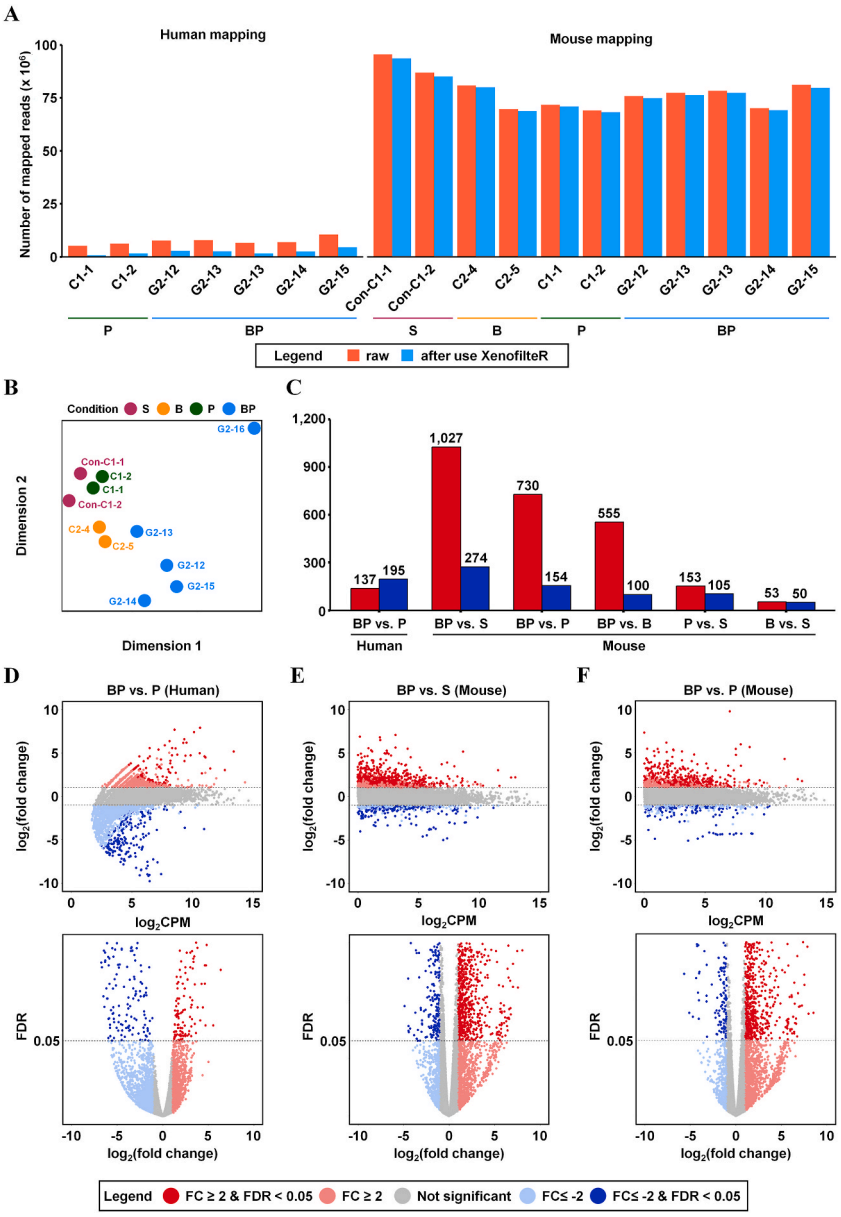

Fig. 5. Gene expression profiles in human-engrafted cells and mouse liver tissue. (A) The number of mapping reads to both human and mouse genomes across 11 samples. The grouped bar plot shows the number of mapping reads, with red bars representing mapping results before using XenofilteR and blue bars indicating results after using XenofilteR. Only the mapping reads after XenofilteR were used to define DEGs. (B) The MDS plot displays sample clustering into four groups: S (red), B (orange), P (green), and BP (sky), illustrating dissimilarities between groups. (C) The number of upregulated and downregulated DEGs between various conditions is shown in a grouped bar plot. DEGs were selected based on a fold change cutoff of >2 or < −2 and a false discovery rate <0.05. (D–F) The MA plot and volcano plot show $\log_2$ gene expression levels on the X-axis and $\log_2$ fold change between groups on the Y-axis. Dots are colored by $\log_2$ fold change and *p*-value.

values <0.05). Therefore, we suggest that mouse liver inflammation is regulated by genes associated with Th1 and Th2 cell differentiation (such as *STAT4*, *IL4R*, and *NFATC1*) and cell cycle (such as *HAUS1*, *CENPU*, *VRK1*, and *KNL1*), respectively.

3.6. *Inflammation and cell adhesion in mouse liver tissue*

In the result of mouse mapping, the upregulated genes were predominantly involved in inflammatory response, regulation of cell motility and cytokine production (Fig. 7A, and Supplementary Table 4–5). The downregulated genes were associated with condensation of prophase chromosomes, metabolic process (Fig. 7A, and Supplementary Table 4–6).

In a previous study, inflammatory mediators such as human IFN-γ and IL-1 family proteins enhanced target tissue injury and

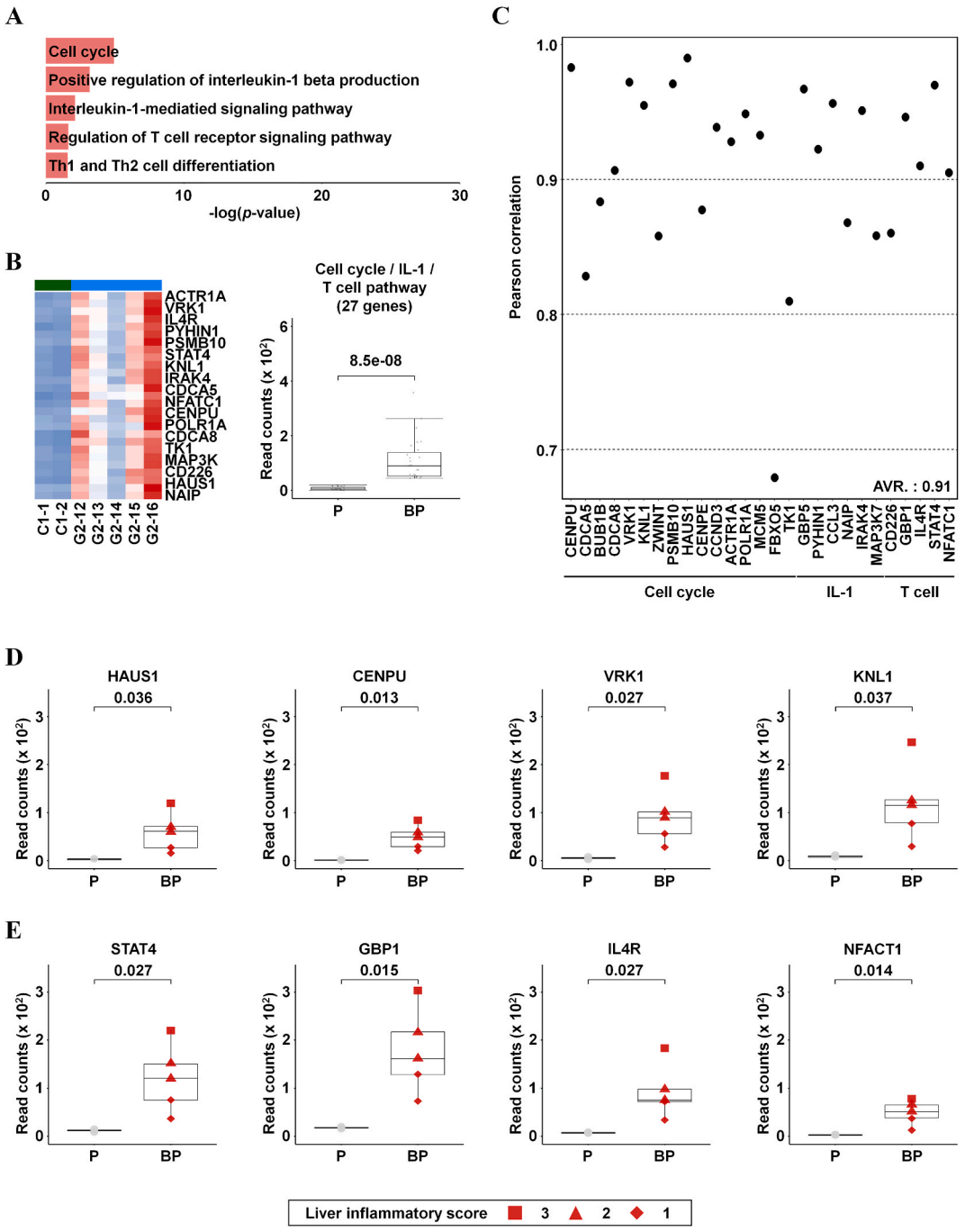

Fig. 6. (A) Highly upregulated pathways in engrafted human PBMCs. The size of bar plot represents -log(*p*-value) derived from Enrichr analysis. (B) A heatmap displays 27 genes from pathways such as Cell cycle, Positive regulation of interleukin-1 beta production, Interleukin-1-mediated signaling pathway, Regulation of T cell receptor signaling pathway, and Th1 and Th2 cell differentiation. Boxplots show results from paired t-tests of enriched genes within each pathway. (C) The scatter plot was generated to show that 27 genes were strong Pearson correlated with liver inflammation scores. (D) Comparison of liver inflammatory scores with the expression (read counts) of genes involved in the cell cycle pathway. (E) Comparison of liver inflammatory scores with the expression of genes in the T cell pathway. In the BP group (n = 5) of panels D and E, inflammatory scores are represented by shapes (square: score of 3, triangle: score of 2, diamond: score of 1). Statistical significance was determined using an unpaired *t*-test. All *p*-values comparing P and BP groups were <0.05.

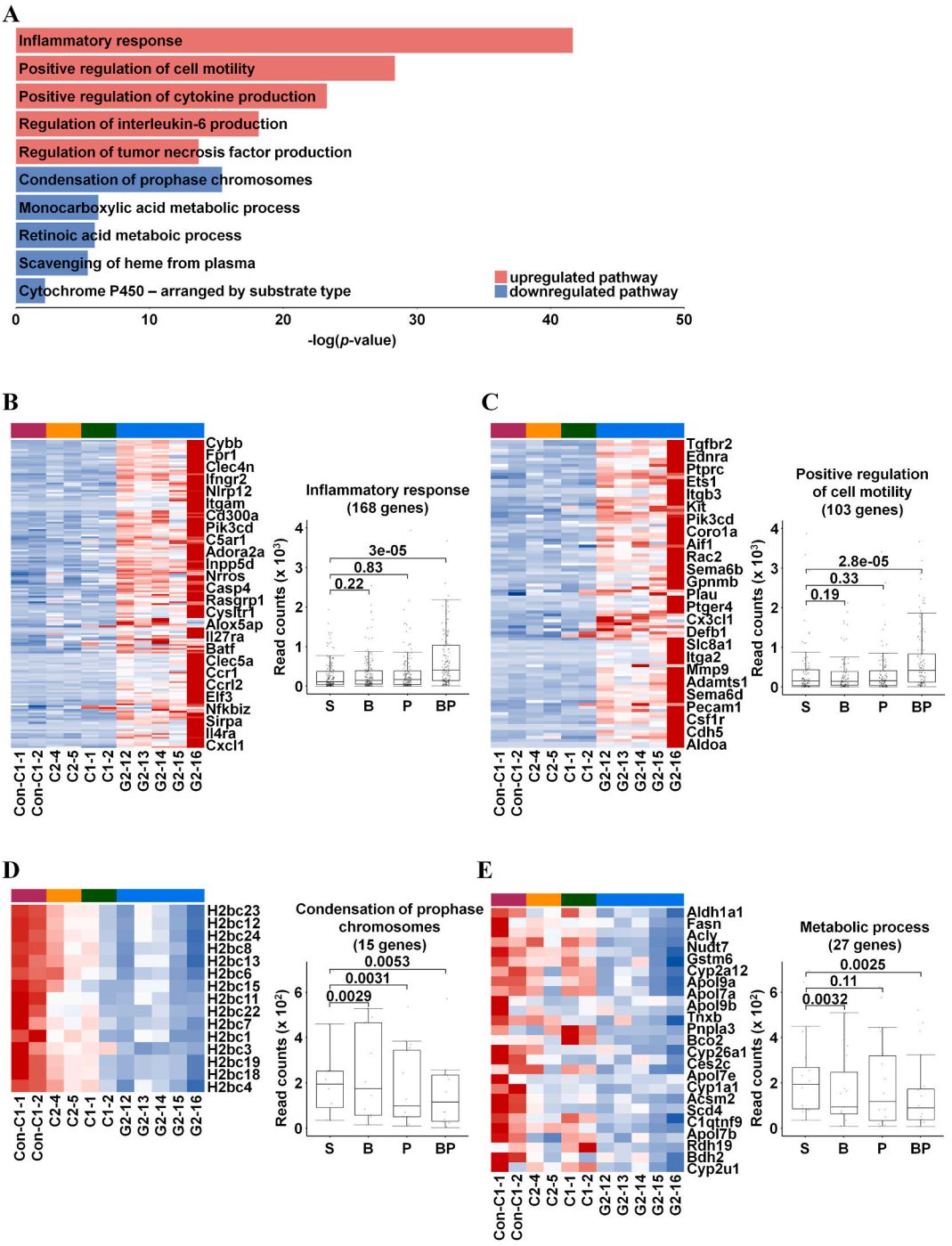

Fig. 7. (A) Upregulated (red) and downregulated (blue) pathways in mouse liver tissue. Pathways were selected based on results from Metascape, represented by -log(p-values). (B) Heatmap and boxplot for the inflammatory response, including 168 genes from the combined pathways: inflammatory response, positive regulation of cytokine production, regulation of interleukin-6 production, and regulation of tumor necrosis factor production. (C) Heatmap and boxplot for the positive regulation of cell motility, including 103 genes. (D) Heatmap and boxplot for the condensation of the prophase chromosome, including 15 genes. (E) Heatmap and boxplot for the metabolic process, combining monocarboxylic acid metabolic process, retinoic acid metabolic process, scavenging of heme from plasma, and cytochrome P450, with 27 genes. Statistical significance was determined using an one-way ANOVA. All *p*-values were <0.05.

destruction caused by GvHD during allogeneic transplantation [31]. In this study, mouse genes associated with IFN-γ (such as interferon-gamma receptor 1 (*Ifngr1*, 1.1), interferon-gamma receptor 2 (*Ifngr2*, 1.0)) and IL-1 (such as interleukin 1 alpha (*Il1a*, 1.3), interleukin 1 receptor-like 2 (*Il1rl2*, 2.4)) were upregulated (Fig. 7B–Supplementary Table 3). Interestingly, upregulated mouse genes associated with the TNF superfamily (e.g., *Tnf*, *Tnfaip3*, *Tnfsf12a*, *Tnfrsf21*) and IL-6 (e.g., *Il6ra*) were also identified, similar to the results from human mapping (see Supplementary Table 4–1).

In the mouse liver of BP group, there was a significant upregulation of adhesion molecules, including intercellular adhesion molecule 1 (*Icam1*, $\log_2$FC = 2.3), intercellular adhesion molecule 2 (*Icam2*, 1.5), vascular cell adhesion molecule 1 (*Vcam1*, 1.6), and endothelin-1 type A receptor (*Ednra*, 1.8) was observed (Fig. 7C–Supplementary Table 4-2 and 4-5). Cell adhesion molecules play a critical role in allograft rejection, and antigen recognition results in leukocyte migration around damaged tissue, and leukocyte-induced tissue injury [32]. *Icam* and *Vcam*, which are expressed on the endothelium, play important roles in the migration of leukocytes into damaged tissue during engrafted T-cell attacks in xenogeneic GvHD [33]. Therefore, our result suggested that activated human T cells regulate cell adhesion molecules (*Icam*, *Vcam*, *Ednra*), leading to liver damage by infiltrated cells producing chemokines and cytokines (*Ccr*, *Il1a*, and *Tgfb*).

In mouse mapping results, the BP group showed downregulation of chromosome-related genes associated with initial condensation of chromosomes during the prophase, such as H2A clustered histone 18 (*H2ac18*, $\log_2$FC = −1.4) and H2B clustered histone 3 (*H2bc3*, -3.4) (Fig. 7D and Supplementary Table 4–2). Notably, previous studies have identified exogenous proteins, such as FSAP, DNase I, and complement component C1q, as potential mediators of chromatin loss and subsequent necrosis [34]. Further, the BP group showed downregulation of monocarboxylic acid and retinoic acid metabolic processes (fatty acid synthase (*Fasn*), retinol dehydrogenase 19

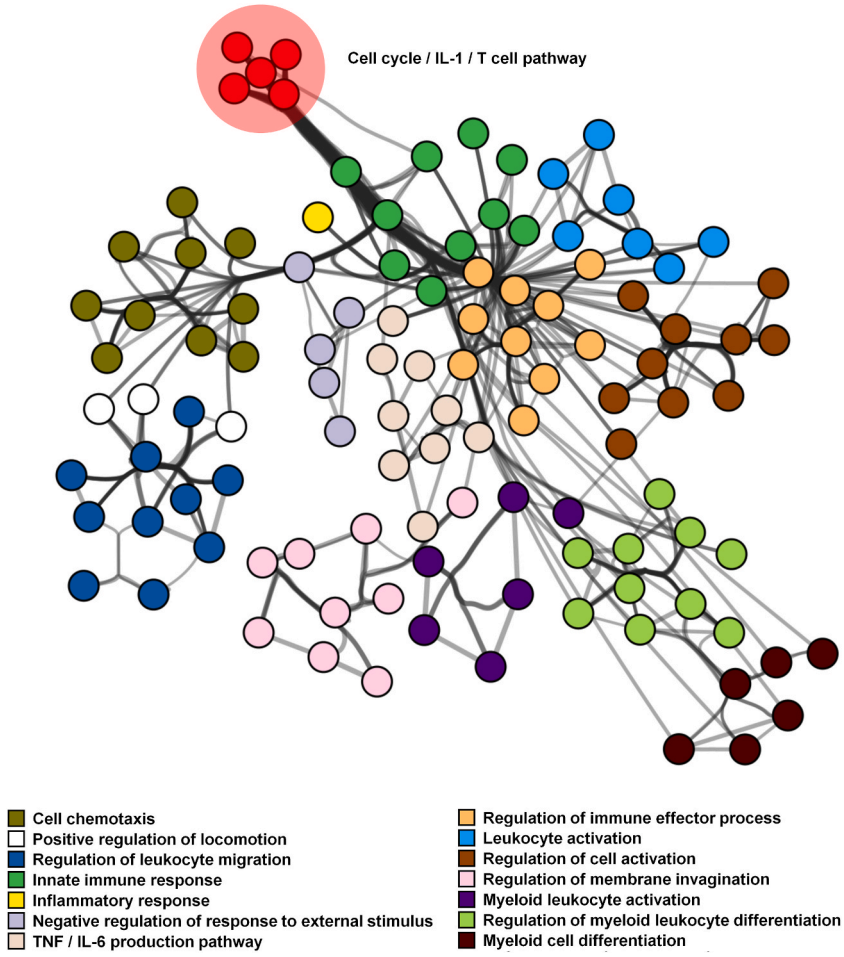

Fig. 8. Pathway network of engrafted human PBMCs and mouse cells. Interaction between human peripheral PBMCs and the host mouse can be observed. Each pathway is represented by nodes, and the strength of the interaction among the pathways was indicated by the thickness of the edges. Each node is colored based on the values calculated using Metascape. Pathways with similar functions are colored in the same color: Cell chemotaxis (olive), Positive regulation of locomotion (white), Regulation of leukocyte migration (blue), Innate immune response (green), Inflammatory response (yellow), Negative regulation of response to external stimulus (lavender), TNF/IL-6 production pathway (beige), Regulation of immune effector process (orange), Leukocyte activation (sky blue), Regulation of cell activation (brown), Regulation of membrane invagination (purple), Myeloid leukocyte activation (indigo), Regulation of myeloid leukocyte differentiation (lime green), Myeloid cell differentiation (maroon).

(*Rdh19*), and stearoyl-coenzyme A desaturase 4 (*Scd4*)), and cytochrome P450 (*Cyp1a1*, *Cyp2a12*, and *Cyp26a1*) (Fig. 7E and Supplementary Table 4–2). Dysfunction in metabolism and liver enzymes can indicate liver damage, as observed in hepatic aGvHD. From the data obtained from Fig. 7, we suggest that liver damage may be regulated by genes associated with chromatin compact (*H2ac18* and *H2bc3*) and fatty acid/steroid metabolism (*Fasn*, *Rdh19*, and *Scd4*).

3.7. Human T cells influencing Tnf/Il6 pathways associated with mouse liver damage

Network analysis was performed using Metascape to understand the interspecies interactions between biological pathways. The human five pathways, including Th1 and Th2 cell differentiation, T cell receptor signaling pathway, IL-1 pathways, and cell cycle (Fig. 6A and Supplementary Table 4–3), were found to be interconnected in the inflammation-related pathways of the mouse, specifically in the inflammatory response, TNF/IL-6 production pathway, and cell trafficking via chemotaxis (Fig. 8). The interconnection in the network was constructed using shared ten genes from both the human and mouse genomes (Supplementary Table 4–7). Following the engraftment of human T cells (illustrated in red), these were observed to interact with the activation of mouse immune cells (shown in green), leading to the upregulation of immune effector processes (depicted in orange) (Fig. 8). The observed necrosis (beige) and leukocyte migration (blue) were identified as direct consequences of the inflammatory response in mouse cells.

Therefore, human T cell differentiation and signaling genes (*CD226*, *GBP1*, *STAT4*, *IL4R*, and *NFACT1*) could trigger a cascade of biological events, including the migration of immune cells (*Icam*, *Vcam*, and *Ednra*) and dysfunction of histone and metabolism (*H2ac18*, *H2bc3*, *Fasn*, *Rdh19*, and *Scd4*) in mice, ultimately leading to liver damage. In addition, the response to external stimuli by human T cells led to the upregulation of genes involved in the TNF superfamily and IL-6 pathways in mouse liver cells, accompanied by hepatocyte necrosis. Considering the cross-reactivity between these human cytokines and their respective mouse receptors [11], we suggest that TNF and IL-6 may upregulate the mouse TNF/IL-6 pathway, leading to liver damage in mice under xenogeneic GvHD.

4. Discussion

In this study, acute and xenogeneic GvHD was induced in NSG mice by conditioning with busulfan, followed by human peripheral PBMC administration [10,11]. Clinical signs of GvHD observed in this study, including weight loss, changes in posture, reduced activity, and altered fur texture, are consistent with those reported in previous studies on allogeneic and xenogeneic rodent models [17, 24].

In the BP group, 2.4- and 4.3-fold increased AST and ALT amounts were determined compared to those in the P group, respectively. These results are similar to those reported by Rhodes et al., who observed increased serum enzyme concentrations in a patient with hepatic GvHD following allogeneic transplantation [35]. Engraftment of hCD45+ leukocytes (59 %) with dominant T cells including $CD4^+$ and $CD8^+$ cells, was found in this study. A viability dye was not used for flow cytometry, which is a limitation of this study. Ali et al. reported that highly engrafted T cells may contribute to the severity of GvHD in a human PBMC-engrafted mouse model [17]. The major hCD4+ T cell-dependent cascade is associated with Th1 rather than Th2 cells in an aGvHD mouse model [16]. In this study, human *STAT4, IL4R,* and *NFACT1* genes included in Th1 and Th2 cell differentiation were overexpressed in the BP group compared to those in the P group. These results imply that *STAT4* and Nuclear Factor of Activated T cells 1 (*NFACT1*) may lead to the differentiation of engrafted human T cell and may induce T cell activation by T cell receptor signaling pathways including *CD226* and *GBP1*. The differentiation from naïve T cells to Th1 cells mediates tissue damage through the activation of cytotoxic $CD8^+$ T cells [3]. Therefore, we concluded that Th1 cytokine production including IL-1 pathway (*CCL3, NAIP,* and *IRAK4*) may be associated with the clinical signs of GvHD in the BP group. This study focused on the T cells that were most abundantly engrafted; therefore, additional experiments are needed to explore the role of other immune cells in human PBMC-engrafted mice suffering from GvHD. In addition, several cell cycle-related genes in human genes, including *CDCA5, CDCA8, MCM5, KNL1, BUB1B, FBXO5,* and *CENPE*, have been implicated in modulating T cell activity and infiltration in various contexts [36–38]. The increased expression of these genes may promote T cell proliferation, survival, and migratory capabilities, potentially facilitating their extravasation and infiltration into the mouse liver parenchyma. In patients who develop liver dysfunction after hematopoietic cell transplantation, hepatic pathological features include infiltrated lymphocytes around the portal tract, damaged bile ducts, and deposition of eosinophilic materials. In addition, bile duct and portal fibrosis have been observed in patients with cGvHD [20]. A damaged bile duct with overlapping nuclei was detected in the BP group, but hepatocellular cholestasis associated with GvHD was not observed [39]. Fujii et al. reported that infiltrated human $CD68^+$ macrophages around the bile duct were correlated with the severity of liver damage including bile duct inflammation, ductopenia, and periductal fibrosis [40]. Therefore, infiltrated Kupffer cells may also be correlated with bile duct proliferation in the BP group suffering from GvHD.

Predicting the severity of GvHD is difficult for patients. Interestingly, the inflammatory score, regarded as the severity of GvHD, was increased with the upregulation of human genes associated with Th1 and Th2 cell differentiation (*STAT4, IL4R,* and *NFACT1*), T cell receptor signaling pathway (*CD226* and *GBP1*), IL-1 pathway (*CCL3, NAIP,* and *IRAK4*), cell cycle (*CDCA5, CDCA8, MCM5, KNL1, BUB1B, FBXO5,* and *CENPE*). The Pearson correlation score between human upregulated genes associated and mouse inflammatory scores showed an average of 0.91. Our findings suggest that their upregulation in the context of GVHD may provide valuable insights into the disease's pathophysiology and could potentially serve as biomarkers when GVHD clinical symptoms manifest.

Infiltrating immune cells originating from both mice and humans were detected around the veins in the BP group. Ichiba et al. found changes in genes associated with leukocyte trafficking in mice with hepatic GvHD after allogeneic bone marrow transplantation, suggesting that VCAM-1 may play a principal role in the migration of leukocytes [33]. ICAM-1 and ICAM-2 proteins are also intercellular adhesion molecules associated with leukocyte migration to tissues in allogeneic transplantation models [41]. Mouse cell

trafficking-related genes, such as *Icam1* ($log_2FC = 2.3$), *Icam2* (1.5), and *Vcam1* (1.6), were upregulated in the BP group compared to those in the S group. Endothelial cells normally express low levels of cell adhesion molecules; however, inflammatory stimuli in endothelial cells induce upregulation of ICAM-1 and VCAM-1 [41]. Therefore, we suggest that mouse cell adhesion molecules may contribute to the infiltration of leukocytes and Kupffer cells in the inflamed liver caused by aGvHD in the xenogeneic transplantation model.

The TNF superfamily is associated with apoptosis or necrosis in GvHD. In mice with allogeneic transplantation, weight loss and mortality caused by GvHD were mediated by TNF-α. Indeed, anti-TNF-α treatment diminishes the pathological features of GvHD, such as focal necrosis of the spleen [42]. We also found that mouse respective receptor superfamily, including *Tnfaip8* (1.6), *Tnfrsf12a* (2.3), *Tnfrsf10b* (2.1), and *Tnfrsf21* (1.7), were upregulated in necrotic livers caused by aGvHD in our model.

IFN-γ can induce apoptosis and inhibit cell cycle progression in hepatocytes [43]. In this study, the expression of mouse *Ifngr1*and *Ifngr2* increased two-fold in the BP group compared to the S group (Supplementary Table 4–2). Considering the absence of both upregulated human genes and the species cross-reactivity of IFN-γ, it is suggested that IFN-γ originating from mouse cells, rather than human cells, may contribute to liver damage through hepatocyte apoptosis.

Increased amounts of the IL-1 family have been observed in patients with GvHD, thereby IL-1 family receptor antagonists have been proposed as novel therapeutics to prevent GvHD-mediated death or symptoms. However, treatment with an IL-1 family receptor antagonist did not ameliorate GvHD or reduce mortality [44]. Unlike IFN-γ and the TNF superfamily, the role of the IL-1 family in liver necrosis or apoptosis in the aGvHD model remains unclear [45]. Although no upregulated human genes associated with IL-1 were detected in the BP group, IL-1 pathways were upregulated in human genes. In addition, mouse interleukin 1 alpha (*Il1a*, 1.3) and interleukin 1 receptor-like 2 (*Il1rl2*, 2.4) were upregulated. Understanding the origin and mechanism of IL-1 in GvHD is crucial for the development of GvHD therapies.

In this study, a humanized mouse model of acute graft-versus-host disease (aGvHD) was established, revealing significant human T cell activation and liver inflammation. Gene expression analysis showed upregulation of cell activation and glucose metabolism pathways in human T cells, with notable downregulation of chromosome condensation and lipid metabolism in mouse liver cells. The model also suggest that activated human T cells contribute to liver damage via inflammatory and metabolic pathways, which are accompanied by elevated levels of cell adhesion molecules and inflammatory cytokines in mice. This research is the first to report interspecies transcriptome analysis of human T cells and mouse liver inflammation in xenografic GvHD. It offers new insights into the disease mechanism and potentially provides novel therapeutic strategies for GvHD.

CRediT authorship contribution statement

Seo Yule Jeong: Writing – original draft, Investigation, Data curation. **Duhyeon Park:** Visualization, Investigation, Data curation. **Tamina Park:** Writing – original draft, Visualization, Formal analysis, Data curation. **Ji-Seok Han:** Writing – original draft, Investigation, Formal analysis. **Jungyun Lee:** Validation, Data curation. **Chang Hoon Choi:** Methodology, Investigation. **Minseong Jo:** Formal analysis, Data curation. **Yu Bin Lee:** Data curation. **Mi-lang Kyun:** Data curation. **Myeongjin Choi:** Writing – review & editing, Writing – original draft, Supervision, Investigation, Formal analysis, Data curation. **Daeui Park:** Writing – original draft, Supervision, Investigation, Data curation. **Kyoung-Sik Moon:** Writing – review & editing, Supervision, Project administration, Data curation.

Ethical approval

The studies involving mice were reviewed and approved by the Institutional Animal Care and Use Committee (IACUC No. 2112–0079, Korea Institute of Toxicology). This study was carried out in compliance with the ARRIVE guidelines.

Data availability statement

The datasets used in this study are available under BioProject accession number PRJNA1013270. The reviewer link is available at

https://dataview.ncbi.nlm.nih.gov/object/PRJNA1013270?reviewer=l7glkdm7ehdcop2mdo388ole30.

Funding statement

This work was supported by the Korea Institute of Toxicology, Republic of Korea (Grant No. 2710008773).

Declaration of competing interest

The authors declare that they have no known competing financial interests or personal relationships that could have appeared to influence the work reported in this paper.

Acknowledgements

None.

Appendix A. Supplementary data

Supplementary data to this article can be found online at https://doi.org/10.1016/j.heliyon.2024.e40559.

References

[1] A. Elhage, C. Sligar, P. Cuthbertson, D. Watson, R. Sluyter, Insights into mechanisms of graft-versus-host disease through humanised mouse models, Biosci. Rep. 42 (9) (2022) BSR20211986, https://doi.org/10.1042/BSR20211986.

[2] G. Ehx, J. Somja, H. Warnatz, C. Ritacco, M. Hannon, L. Delens, G. Fransolet, P. Delvenne, J. Muller, Y. Beguin, H. Lehrach, L. Belle, S. Humblet-Baron, F. Baron, Xenogeneic graft-versus-host disease in humanized NSG and NSG-HLA-A2/HHD mice, Front. Immunol. 9 (2018) 1943, https://doi.org/10.3389/fimmu.2018.01943.

[3] S. Ghimire, D. Weber, E. Mavin, X.N. Wang, A.M. Dickinson, E. Holler, Pathophysiology of GvHD and other HSCT-related major complications, Front. Immunol. 8 (2017) 79, https://doi.org/10.3389/FIMMU.2017.00079.

[4] R. Zeiser, B.R. Blazar, Acute graft-versus-host disease biologic process, prevention and therapy, N. Engl. J. Med. 377 (22) (2017) 2167–2179, https://doi.org/10.1056/NEJMra1609337.

[5] C.K. Min, The pathophysiology of chronic graft-versus-host disease: the unveiling of an enigma, Korean J Hematol 46 (2) (2011) 80–87, https://doi.org/10.5045/kjh.2011.46.2.80.

[6] S. Paczesny, Discovery and validation of graft-versus-host disease biomarkers, Blood 121 (4) (2013) 585–594, https://doi.org/10.1182/blood-2012-08-355990.

[7] J. Chen, S. Liao, Z. Xiao, Q. Pan, X. Wang, K. Shen, S. Wang, L. Yang, F. Guo, H.F. Liu, Q. Pan, The development and improvement of immunodeficient mice and humanized immune system mouse models, Front. Immunol. 13 (2022) 1007579, https://doi.org/10.3389/FIMMU.2022.1007579.

[8] Y. Ishikawa, T. Usui, A. Shiomi, M. Shimizu, K. Murakami, T. Mimori, Functional engraftment of human peripheral T and B cells and sustained production of autoantibodies in NOD/LtSzscid/IL-2Rγ −/− mice, Eur. J. Immunol. 44 (11) (2014) 3453–3463, https://doi.org/10.1002/eji.201444729.

[9] Y. Ka, I. Katano, E. Nishinaka, J. Welcker, M. Mochizuki, K. Kawai, M. Goto, K. Tomiyama, T. Ogura, T. Yamamoto, M. Ito, R. Ito, R. Takahashi, Improved engraftment of human peripheral blood mononuclear cells in NOG MHC double knockout mice generated using CRISPR/Cas9, Immunol. Lett. 229 (2021) 55–61, https://doi.org/10.1016/j.imlet.2020.11.011.

[10] L.D. Shultz, P.A. Schweitzer, S.W. Christianson, B. Gott, I.B. Schweitzer, B. Tennent, S. McKenna, L. Mobraaten, T. V Rajan, D.L. Greiner, Multiple defects in innate and adaptive immunologic function in NOD/LtSz-scid mice, J. Immunol. 154 (1) (1995) 180–191, https://doi.org/10.4049/JIMMUNOL.154.1.180.

[11] W.F. Garcia-Beltran, D.T. Claiborne, C.R. Maldini, M. Phelps, V. Vrbanac, M.E. Karpel, K.L. Krupp, K.A. Power, C.L. Boutwell, A.B. Balazs, A.M. Tager, M. Altfeld, T.M. Allen, Innate immune reconstitution in humanized bone marrow-liver-thymus (HuBLT) mice governs adaptive cellular immune function and responses to HIV-1 infection, Front. Immunol. 12 (2021) 667393, https://doi.org/10.3389/fimmu.2021.667393.

[12] M.N. Bouchlaka, A.B. Moffitt, J. Kim, J.A. Kink, D.D. Bloom, C. Love, S. Dave, P. Hematti, C.M. Capitini, Human mesenchymal stem cell–educated macrophages are a distinct high IL-6–producing subset that confer protection in graft-versus-host-disease and radiation injury models, Biol. Blood Marrow Transplant. 23 (6) (2017) 897–905, https://doi.org/10.1016/j.bbmt.2017.02.018.

[13] J. Hayakawa, M.M. Hsieh, N. Uchida, O. Phang, J.F. Tisdale, Busulfan produces efficient human cell engraftment in NOD/LtSz-Scid IL2Rgamma(null) mice, Stem Cell. 27 (1) (2009) 175–182, https://doi.org/10.1634/stemcells.2008-0583.

[14] S. Schwarte, M. Bremer, J. Fruehauf, Y. Sorge, S. Skubich, M.W. Hoffmann, Radiation protocols determine acute graft-versus-host disease incidence after allogeneic bone marrow transplantation in murine models, Int. J. Radiat. Biol. 83 (9) (2007) 625–636, https://doi.org/10.1080/09553000701534572.

[15] M. Haque, D.A. Boardman, A.J. Lam, K.N. MacDonald, L. Sanderink, Q. Huang, V.C.W. Fung, S. Ivison, M. Mojibian, M.K. Levings, Modelling graft-versus-host disease in mice using human peripheral blood mononuclear cells, Bio Protoc 12 (23) (2022) e4566, https://doi.org/10.21769/BioProtoc.4566.

[16] M.A. Schroeder, J.F. DiPersio, Mouse models of graft-versus-host disease: advances and limitations, Dis Model Mech 4 (3) (2011) 318–333, https://doi.org/10.1242/dmm.006668.

[17] N. Ali, B. Flutter, R. Sanchez Rodriguez, E. Sharif-Paghaleh, L.D. Barber, G. Lombardi, F.O. Nestle, Xenogeneic graft-versus-host-disease in NOD-scid IL-2rγnull mice display a T-effector memory phenotype, PLoS One 7 (8) (2012) e44219, https://doi.org/10.1371/journal.pone.0044219.

[18] Y. Tago, C. Kobayashi, M. Ogura, J. Wada, S. Yamaguchi, T. Yamaguchi, M. Hayashi, T. Nakaishi, H. Kubo, Y. Ueda, Human amnion-derived mesenchymal stem cells attenuate xenogeneic graft-versus-host disease by preventing T cell activation and proliferation, Sci. Rep. 11 (1) (2021) 2406, https://doi.org/10.1038/s41598-021-81916-y.

[19] R.M. Saliba, M. de Lima, S. Giralt, B. Andersson, I.F. Khouri, C. Hosing, S. Ghosh, J. Neumann, Y. Hsu, J. De Jesus, M.H. Qazilbash, R.E. Champlin, D.R. Couriel, Hyperacute GVHD: risk factors, outcomes, and clinical implications, Blood 109 (7) (2007) 2751–2758, https://doi.org/10.1182/blood-2006-07-034348.

[20] K.E. Matsukuma, D. Wei, K. Sun, R. Ramsamooj, M. Chen, Diagnosis and differential diagnosis of hepatic graft versus host disease (GVHD), J. Gastrointest. Oncol. 7 (Suppl 1) (2016) S21–S31, https://doi.org/10.3978/j.issn.2078-6891.2015.036.

[21] M. Weber, P. Stein, S. Prüfer, B. Rudolph, A. Kreft, E. Schmitt, T. Bopp, A. Roers, H. Schild, S. Fillatreau, M.P. Radsak, Donor and host B cell-derived IL-10 contributes to suppression of graft-versus-host disease, Eur. J. Immunol. 44 (6) (2014) 1857–1865, https://doi.org/10.1002/eji.201344081.

[22] S.W. Choi, P. Stiff, K. Cooke, J.L.M. Ferrara, T. Braun, C. Kitko, P. Reddy, G. Yanik, S. Mineishi, S. Paczesny, D. Hanauer, A. Pawarode, E. Peres, T. Rodriguez, S. Smith, J.E. Levine, TNF-inhibition with etanercept for graft-versus-host disease prevention in high-risk HCT: lower TNFR1 levels correlate with better outcomes, Biol. Blood Marrow Transplant. 18 (10) (2012) 1525–1532, https://doi.org/10.1016/j.bbmt.2012.03.013.

[23] Y. Ye, L. Ricard, N. Stocker, M. Mohty, B. Gaugler, F. Malard, A novel mouse model of acute graft-versus-host disease based on chemotherapy conditioning and G-CSF mobilized graft, Bone Marrow Transplant. 55 (3) (2020) 570–577, https://doi.org/10.1038/s41409-019-0700-4.

[24] H.Y. Lai, T.Y. Chou, C.H. Tzeng, O.K.S. Lee, Cytokine profiles in various graft-versus-host disease target organs following hematopoietic stem cell transplantation, Cell Transplant. 21 (9) (2012) 2033–2045, https://doi.org/10.3727/096368912X653110.

[25] A. Dobin, C.A. Davis, F. Schlesinger, J. Drenkow, C. Zaleski, S. Jha, P. Batut, M. Chaisson, T.R. Gingeras, STAR: ultrafast universal RNA-seq aligner, Bioinformatics 29 (1) (2013) 15–21, https://doi.org/10.1093/bioinformatics/bts635.

[26] R.J.C. Kluin, K. Kemper, T. Kuilman, J.R. de Ruiter, V. Iyer, J.V. Forment, P. Cornelissen-Steijger, I. de Rink, P. ter Brugge, J.Y. Song, S. Klarenbeek, U. McDermott, J. Jonkers, A. Velds, D.J. Adams, D.S. Peeper, O. Krijgsman, XenofilteR: computational deconvolution of mouse and human reads in tumor xenograft sequence data, BMC Bioinf. 19 (1) (2018) 366, https://doi.org/10.1186/s12859-018-2353-5.

[27] Y. Liao, G.K. Smyth, W. Shi, featureCounts: an efficient general purpose program for assigning sequence reads to genomic features, Bioinformatics 30 (7) (2014) 923–930, https://doi.org/10.1093/bioinformatics/btt656.

[28] M.D. Robinson, D.J. McCarthy, G.K. Smyth, edgeR: a Bioconductor package for differential expression analysis of digital gene expression data, Bioinformatics 26 (1) (2010) 139–140, https://doi.org/10.1093/bioinformatics/btp616.

[29] Y. Zhou, B. Zhou, L. Pache, M. Chang, A.H. Khodabakhshi, O. Tanaseichuk, C. Benner, S.K. Chanda, Metascape provides a biologist-oriented resource for the analysis of systems-level datasets, Nat. Commun. 10 (1) (2019) 1523, https://doi.org/10.1038/s41467-019-09234-6.

[30] M.V. Kuleshov, M.R. Jones, A.D. Rouillard, N.F. Fernandez, Q. Duan, Z. Wang, S. Koplev, S.L. Jenkins, K.M. Jagodnik, A. Lachmann, M.G. McDermott, C. D. Monteiro, G.W. Gundersen, A. Maayan, Enrichr: a comprehensive gene set enrichment analysis web server 2016 update, Nucleic Acids Res. 44 (W1) (2016) W90–W97, https://doi.org/10.1093/nar/gkw377.

[31] J.E. Levine, Implications of TNF-α in the pathogenesis and management of GVHD, Int. J. Hematol. 93 (5) (2011) 571–577, https://doi.org/10.1007/s12185-011-0803-1.

[32] K.O. Schowengerdt, J.Y. Zhu, S.M. Stepkowski, Y. Tu, M.L. Entman, C.M. Ballantyne, Cardiac allograft survival in mice deficient in intercellular adhesion molecule-1, Circulation 92 (1) (1995) 82–87, https://doi.org/10.1161/01.cir.92.1.82.
[33] T. Ichiba, T. Teshima, R. Kuick, D.E. Misek, C. Liu, Y. Takada, Y. Maeda, P. Reddy, D.L. Williams, S.M. Hanash, J.L.M. Ferrara, Early changes in gene expression profiles of hepatic GVHD uncovered by oligonucleotide microarrays, Blood 102 (2) (2003) 763–771, https://doi.org/10.1182/blood-2002-09-2748.
[34] M. Sachet, Y.Y. Liang, R. Oehler, The immune response to secondary necrotic cells, Apoptosis 22 (10) (2017) 1189–1204, https://doi.org/10.1007/s10495-017-1413-z.
[35] S.Y. Ma, W.Y. Au, I.O.L. Ng, A.K.W. Lie, A.Y.H. Leung, R. Liang, G.K.K. Lau, Y.L. Kwong, Hepatitic graft-versus-host disease after hematopoietic stem cell transplantation: clinicopathologic features and prognostic implication, Transplantation 77 (8) (2004) 1252–1259, https://doi.org/10.1097/01.tp.0000120383.30088.a4.
[36] H. Hu, M. Umair, S.A. Khan, A.I. Sani, S. Iqbal, F. Khalid, R. Sultan, M.A. Abdel-Maksoud, A. Mubarak, T.M. Dawoud, A. Malik, I.A. Saleh, A.A. Al Amri, N. K. Algarzae, A.S. Kodous, Y. Hameed, CDCA8, a mitosis-related gene, as a prospective pan-cancer biomarker: implications for survival prognosis and oncogenic immunology, Am J Transl Res 16 (2) (2024) 432–445, https://doi.org/10.62347/WSEF7878.
[37] Y. Zhang, Q. Ji, J. Wang, Y. Dong, M. Pang, S. Fu, Y. Wei, Q. Zhu, High expression of KNL1 in prostate adenocarcinoma is associated with poor prognosis and immune infiltration, Front. Genet. 13 (2023) 1100787, https://doi.org/10.3389/fgene.2022.1100787.
[38] P. Liu, X. Wang, L. Pan, B. Han, Z. He, Prognostic significance and immunological role of FBXO5 in human cancers: a systematic pan-cancer analysis, Front. Immunol. 13 (2022) 901784, https://doi.org/10.3389/fimmu.2022.901784.
[39] S.-Y. Joo, K.-A. Cho, Y.-J. Jung, H.-S. Kim, S.-Y. Park, Y.-B. Choi, K.-M. Hong, S.-Y. Woo, J.-Y. Seoh, S.J. Cho, K.-H. Ryu, Mesenchymal stromal cells inhibit graft-versus-host disease of mice in a dose-dependent manner, Cytotherapy 12 (3) (2010) 361–370, https://doi.org/10.3109/14653240903502712.
[40] H. Fujii, Z.-J. Luo, H.J. Kim, S. Newbigging, A. Gassas, A. Keating, R.M. Egeler, Humanized chronic graft-versus-host disease in NOD-SCID il2rγ-/- (NSG) mice with G-CSF-mobilized peripheral blood mononuclear cells following cyclophosphamide and total body irradiation, PLoS One 10 (7) (2015) e0133216, https://doi.org/10.1371/journal.pone.0133216.
[41] S.-R. Kim, Y.-H. Bae, S.-K. Bae, K.-S. Choi, K.-H. Yoon, T.H. Koo, H.-O. Jang, I. Yun, K.-W. Kim, Y.-G. Kwon, M.-A. Yoo, M.-K. Bae, Visfatin enhances ICAM-1 and VCAM-1 expression through ROS-dependent NF-kappaB activation in endothelial cells, Biochim. Biophys. Acta 1783 (5) (2008) 886–895, https://doi.org/10.1016/j.bbamcr.2008.01.004.
[42] K. Hattori, T. Hirano, H. Miyajima, N. Yamakawa, M. Tateno, K. Oshimi, N. Kayagaki, H. Yagita, K. Okumura, Differential effects of anti-Fas ligand and anti-tumor necrosis factor alpha antibodies on acute graft-versus-host disease pathologies, Blood 91 (11) (1998) 4051–4055, https://doi.org/10.1182/blood.V91.11.4051.
[43] C.J. Horras, C.L. Lamb, K.A. Mitchell, Regulation of hepatocyte fate by interferon-γ, Review Cytokine Growth Factor Rev 22 (1) (2011) 35–43, https://doi.org/10.1016/j.cytogfr.2011.01.001.
[44] J.H. Antin, D. Weisdorf, D. Neuberg, R. Nicklow, S. Clouthier, S.J. Lee, E. Alyea, C. McGarigle, B.R. Blazar, S. Sonis, R.J. Soiffer, J.L.M. Ferrara, Interleukin-1 blockade does not prevent acute graft-versus-host disease: results of a randomized, double-blind, placebo-controlled trial of interleukin-1 receptor antagonist in allogeneic bone marrow transplantation, Blood 100 (10) (2002) 3479–3483, https://doi.org/10.1182/blood-2002-03-0985.
[45] T. Sakurai, G. He, A. Matsuzawa, G.-Y. Yu, S. Maeda, G. Hardiman, M. Karin, Hepatocyte necrosis induced by oxidative stress and IL-1 alpha release mediate carcinogen-induced compensatory proliferation and liver tumorigenesis, Cancer Cell 14 (2) (2008) 156–165, https://doi.org/10.1016/j.ccr.2008.06.016.